Characteristics of a novel biaxial capacitive MEMS accelerometer*

Dong Linxi(董林玺)[1, 2, †], Li Yongjie(李永杰)[1], Yan Haixia(颜海霞)[3], and Sun Lingling(孙玲玲)[1]

(1 Key Laboratory of RF Circuits and System of Ministry of Education, Hangzhou Dianzi University, Hangzhou 310018, China)
(2 State Key Laboratory of Transducer Technology, Chinese Academy of Sciences, Shanghai 200050, China)
(3 Toshiba Hydro-Electro Equipments Company, Hangzhou 311504, China)

Abstract: A novel MEMS accelerometer with grid strip capacitors is developed. The mechanical and electrical noise can be reduced greatly for the novel structure design. ANSOFT-Maxwell software was used to analyze the fringing electric field of the grid strip structure and its effects on the designed accelerometer. The effects of the width, thickness and overlapping width of the grid strip on the sensing capacitance are analyzed by using the ANSOFT-Maxwell software. The results show that the parameters have little effect on the characteristics of the presented accelerometer. The designed accelerometer was fabricated based on deep RIE and silicon–glass bonding processes. The preliminary tested sensitivities are 0.53 pF/g and 0.49 pF/g in the x and y axis directions, respectively. A resonator with grid strip structure was also fabricated whose tested quality factor is 514 in air, which proves that the grid strip structure can reduce mechanical noise.

Key words: MEMS; biaxial accelerometer; capacitor fringe effect; slide-film damping
DOI: 10.1088/1674-4926/31/5/054006 **EEACC:** 2520

1. Introduction

High resolution accelerometers are widely used in assistant navigation, robots, earthquake detection etc. Comb capacitors fabricated by bulk silicon micro processing are the structure mostly used in high resolution accelerometers[1]. The deep RIE process, which is an important process in bulk silicon micro processing, may cause non-parallel plates in the comb capacitor, which affect the resolution and linear work range of the accelerometer[2, 3]. Grid strip structures based on a bulk silicon process were proposed in Refs. [4, 5], which work on slide-film damping so that the accelerometer has a higher resolution in air pressure. Compared with the traditional comb structure, the grid strip structure can eliminate the effect of non-parallel comb capacitors caused by the deep RIE process. It can also sustain a higher detecting voltage while avoiding the pull-in effect and lead to higher resolution.

The detecting theory of the grid strip capacitor is based on the change of overlapping area, which has a high linear work range compared with the comb structure. Since the capacitor plates of the grid strips do not entirely overlap, there is a fringing electric field aside from the overlapping area, which affects the detecting capacitance of the accelerometer. Therefore, it is important to analyze the fringing electric field in the design of MEMS capacitive devices with grid strip structure. A modified capacitance calculation formula was proposed in Ref. [6], which contains fringing electric field analyses. But the formula cannot be used in the grid structure because it cannot precisely predict the capacitance of the grid strip structure. According to the situations above, a method of using an electric-magnetic field analyzing software, ANSOFT-Maxwell, is proposed, which can precisely calculate the capacitance of the grid strip structure. Analyzing the results shows that the parallel plate approximation and modified formula cannot calculate capacitance precisely; that the fringing electric field has an effect on the capacitance of the grid strip structure and that the capacitance changes nonlinearly with the change of overlap width.

2. Theoretical analyses

2.1. Noise analyses

There are two major noise sources for capacitive MEMS accelerometers: mechanical noise and electrical noise. The mechanical noise is caused by the damping movement of air molecules around the physical structure of the accelerometer. According to Gabrielson, the equivalent acceleration of mechanical noise can be expressed by[7]:

$$\bar{a}_{\mathrm{m}} = \sqrt{\frac{4k_{\mathrm{B}}T\omega_{\mathrm{n}}}{mQ}}, \tag{1}$$

where k_{B}, T, ω_{n} are the Boltzmann constant, absolute temperature and natural frequency of the accelerometer, respectively, m is the seismic mass, and Q is the quality factor of the sensor. Compared with squeezed-film damping, slide-film damping usually leads to a smaller damping ratio and a higher Q factor, so it can decrease the mechanical noise of the accelerometer.

Another major noise source is the interface circuit. Modulation and demodulation is a common detecting method for capacitive accelerometers. In this method, high frequency carrier waves with opposite phase are applied on accelerometer capacitors to modulate the acceleration signal, and then the signal is amplified and demodulated. In this situation the electrical noise is determined mainly by the noise in the frond-end

* Project supported by the National Natural Science Foundation of China (No. 60506015) and the Zhejiang Provincial Natural Science Foundation of China (No.Y107105).
† Corresponding author. Email: donglinxi@hdu.edu.cn
Received 3 November 2009, revised manuscript received 7 January 2010

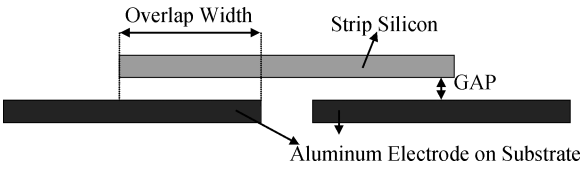

Fig. 1. Schematic figure of grid strip structure.

preamplifier. The electrical noise can be expressed by the following equation[8]:

$$\bar{a}_{\mathrm{e}} = \sqrt{\frac{\alpha}{C + C_{\mathrm{p}} + C_{\mathrm{i}}} \frac{\omega_{\mathrm{n}}^2}{V_{\mathrm{s}}} \bar{v}_{\mathrm{e}}}, \tag{2}$$

where α is the constant related to the sizes of the sensor, C is the sensing capacitance of the sensor, C_{p} is the parasitical capacitance, V_{s} is the voltage of the testing signal, and $\overline{v}_{\mathrm{e}}$ is the voltage of the input noise. Equation (2) shows that the electronic noise can be reduced by increasing the sensing capacitance or amplitude of the electronic testing signal in the capacitive accelerometer design.

The total noise of capacitive accelerometers can be expressed by:

$$\bar{a}_{\mathrm{total}} = \sqrt{\bar{a}_{\mathrm{e}}^2 + \bar{a}_{\mathrm{m}}^2}. \tag{3}$$

From Eq. (3), a conclusion can be drawn that the designed accelerometer has a low mechanical noise since it works on slide-film damping and the electric noise can be reduced through the use of large testing signals and sensing capacitance.

2.2. Working principles

The sensing capacitor of the designed accelerometer is composed of grid strips, including beam-supported proof mass and aluminum electrodes deposited on glass substrate. One silicon grid strip electrode has a counterpart of two aluminum electrodes, forming a differential capacitor structure. A schematic picture is shown in Fig. 1.

The designed accelerometer detects an inertial signal through capacitance changes based on capacitor area change: acceleration causes displacement of proof mass, which leads to area change of sensing capacitors and then capacitance change. When the proof mass has a displacement of Δx in the x-direction, the capacitance change ΔC can be calculated by:

$$\begin{aligned}\Delta C = C_1' - C_2' &= \frac{\varepsilon\varepsilon_0 nl(w + \Delta x)}{d} - \frac{\varepsilon\varepsilon_0 nl(w - \Delta x)}{d} \\ &= \frac{\varepsilon\varepsilon_0 nl}{d} \times 2\Delta x,\end{aligned} \tag{4}$$

where ε is permittivity, n is the number of silicon grid strip electrodes, while l, w and d are overlap length, overlap width and gap between proof mass and substrate, respectively.

When the inertial force and elastic force are in balance:

$$F = ma = k \times \Delta x \Rightarrow \Delta x = ma/k, \tag{5}$$

where k, a and m are the elastic constant, acceleration, and mass of the proof mass respectively. So the relation between capacitance change and acceleration can be expressed by:

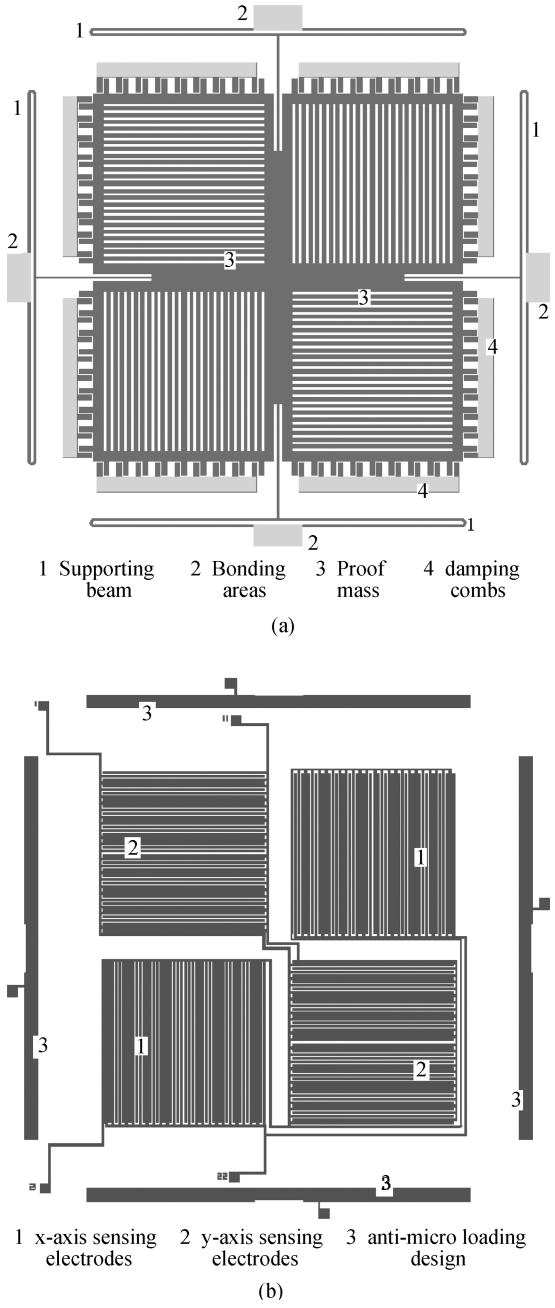

Fig. 2. Accelerometer structure. (a) Silicon proof mass and supporting beam. (b) Aluminum electrodes.

$$\Delta C = \frac{\varepsilon\varepsilon_0 nl}{d} \frac{m}{k} a. \tag{6}$$

When the structure of the accelerometer is fixed, all the parameters in front of a in Eq. (6) are constant, and the relation between capacitance change and acceleration approximates to be linear.

2.3. Structure of the designed accelerometer

The designed accelerometer consists of proof mass, supporting beam, glass substrate, aluminum electrodes etc, as shown in Fig. 2. Damping combs are added in order to adjust the damping of the MEMS accelerometer.

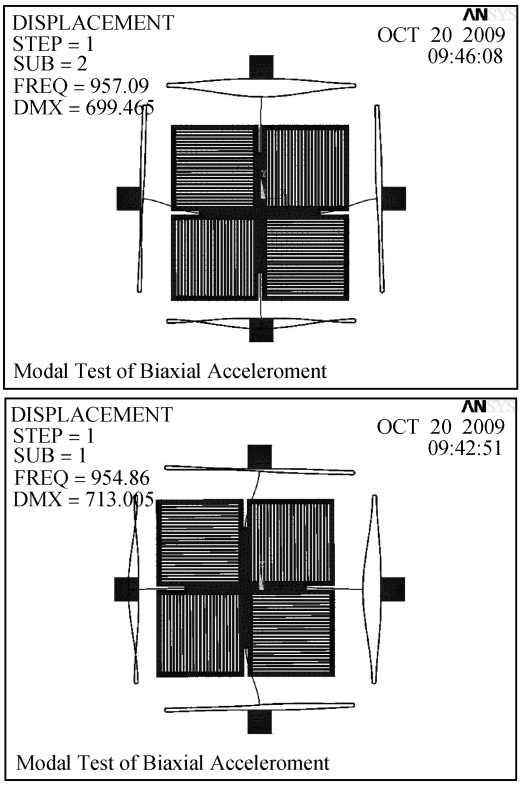

Fig. 3. First and second vibrating modes.

3. Performance of the accelerometer

To verify the structural design of the accelerometer, several analyses including modal analyses, strength analysis and transverse sensitivity analyses were performed by using the FEM software ANSYS.

3.1. Mode analyses

The analytical results are shown in Fig. 3: vibration modes of the first and second modal are translational movement in the y- and x-directions with frequencies of 957 and 955 respectively. When 1 g acceleration is applied in the x- and y-directions respectively, the displacements are both 0.273 μm, so the accelerometer has the same sensitivity in the x- and y-axes.

3.2. Strength analysis

The strength performance of the accelerometer was analyzed to verify if the accelerometer can sustain a large shock. Overloading heaves are designed in both x- and y-directions to protect the accelerometer from damage from large shocks. However, a similar structure cannot be added in the z-axis, leaving the accelerometer unprotected in the z-axis, so the anti-collision performance of the accelerometer depends on the performance in the z-axis. In the analysis, an acceleration of 1000g is applied on the z-axis; the result is shown in Fig. 4. The maximum stress in Fig. 4 is 321 MPa, less than the fracture stress of silicon material i.e. 1.3 GPa[9], which indicates that the accelerometer can sustain a shock acceleration of 1000 g.

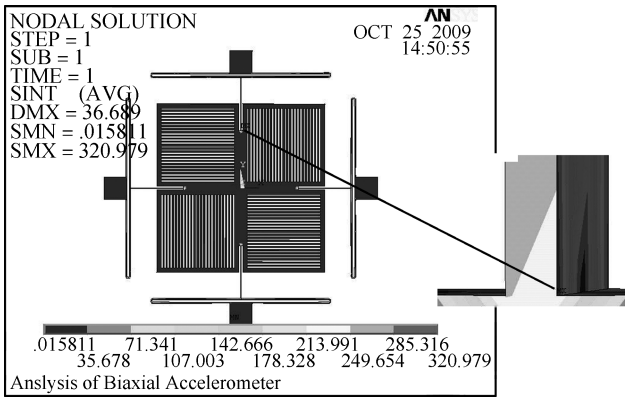

Fig. 4. Strength analysis result.

Table 1. Analytical results of transverse sensitivity.

Acceleration		Δx (μm)	Δy (μm)
$a_x = 1g$	$a_y = 1g$	0.2734	0.2734
$a_x = 2g$	$a_y = 1g$	0.5467	0.2735
$a_z = 1g$	$a_y = 1g$	0.0001	0.2724
$a_z = 2g$	$a_y = 1g$	0.0002	0.2723

3.3. Transverse sensitivity

The transverse sensitivity of the x-axis describes the influence of y- and z-axis acceleration on the x-axis; in this condition, the x-axis output can be expressed by:

$$a_{\text{out}\_x} = S_{xx}a_x + S_{yx}a_y + S_{zx}a_z, \tag{7}$$

where S_{xx}, S_{yx}, S_{zx} are x-axis sensitivities induced by x-, y- and z-axis accelerations respectively and a_x, a_y, a_z are accelerations on x-, y- and z-axes. The analytical results in Table 1 show that $S_{yx} \approx S_{zx} \approx S_{zy} \approx 0$, which indicates that the transverse sensitivity of the accelerometer is 0.

4. Fringing electric field analyses

The analyses on detecting principles in section 2.2 are based on a parallel plate approximation with the assumption that the length and width of the capacitor plates are much larger than plate distance. However, in this paper, the designed grid strip structure cannot fulfill this assumption, and additionally, the designed grid strip structure has non-entirely overlapping plates, so the fringe effect of the grid strip structure should be considered. An electric-magnetic analyzing software, ANSOFT-Maxwell, which uses the FEM method, is used in this paper to analyze the fringe effect of the grid strip capacitance.

4.1. Capacitance change with the change of overlap width

The analyzing model includes a 35×200 μm^2 silicon electrode and 30×200 μm^2 aluminum electrode, and the electric field region shows 100% extension in the x-, y- and z-axes about the electrode size. The capacitance with overlap width from 0 to 23.5 μm is analyzed; the analytical and computational results of the parallel plate approximation and modified parallel approximation are shown in Fig. 5(a), which indicates that there are large errors in the results derived from the parallel plate approximation, according to the analytical results.

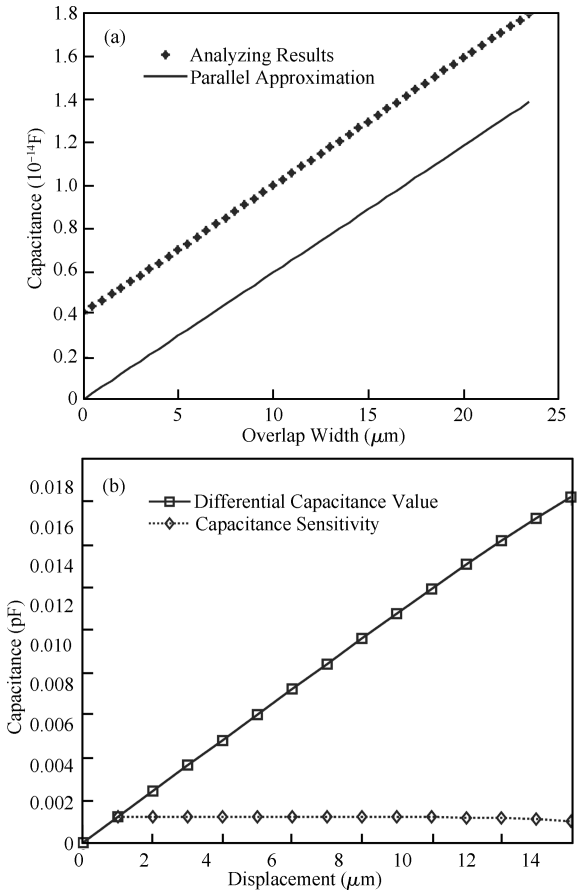

Fig. 5. Capacitance in different overlap widths. (a) Comparison of analyzed and computed capacitance. (b) Differential capacitance changes.

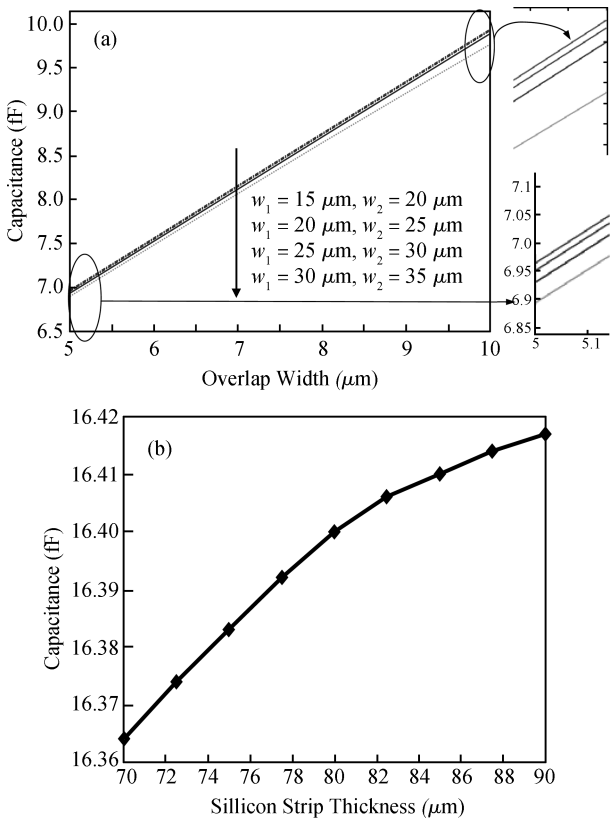

Fig. 6. Analyzed capacitance. (a) Capacitance change of different grid strip widths. (b) Capacitance of different silicon thicknesses.

The differential capacitance change was also analyzed through a model of a 35×200 μm^2 silicon electrode and a pair of 30×200 μm^2 aluminum electrodes with a default overlap width of 15 μm. The results in Fig. 5(b) shows that the capacitance sensitivity of the designed accelerometer decreases nonlinearly with the increase of proof mass displacement; that the capacitance decrease rate is less than 0.3% within 5 μm displacement, which indicates that the accelerometer sensitivity changes linearly within 5 μm displacement, and that the designed accelerometer works linearly within 5 μm proof mass displacement.

4.2. Capacitance in different grid strip widths and thicknesses

According to Eq. (6), when the capacitor area of the accelerometer is fixed, sensitivity increases as the number of grid strips increases. Meanwhile the corresponding fringing effect changes too. Grid strips with a length of 200 μm were analyzed to verify the capacitance difference in different grid strip widths; w_1 and w_2 are the aluminum grid strip width and silicon electrode width respectively. The results in Fig. 6(a) show that capacitance increases with the increase of grid strip width under the same overlap width, and that the increase rate changes from 1.25% to 0.18% while w_1 changes from 15 to 30 μm.

Non-ideal effects of the DRIE process may cause thickness change of the designed structure. Since the capacitance changes with thickness change of the capacitor plates, analyses of the capacitance at different electrode thicknesses are important. A 200×35 μm^2 silicon strip and a 200×30 μm^2 aluminum electrode are employed to analyze capacitance changes with silicon electrode thickness. The designed thickness of silicon strip is 80 μm, so capacitors with a silicon strip thickness from 70 to 90 μm are analyzed to verify the influence of thickness change on capacitance. The results in Fig. 6(b) show that capacitance increases with the increase of silicon thickness. When the thickness changes 10 μm from 80 μm the increase and decrease rates are 0.1% and 0.2%, indicating that for the designed capacitor structure the thickness change caused by non-ideal effects of the DRIE process can be neglected.

5. Accelerometer fabrication and primary test

To verify the design, the accelerometer was fabricated by using a bulk silicon process. The proof mass and substrate materials are N-type (100) double-sided polished silicon and Pyrex glass respectively. The fabricating process includes deep RIE, silicon–glass bonding, lithography, sputtering etc. The major processes are shown in Fig. 7.

When the accelerometer is being fabricated by the DRIE process, a micro loading effect occurs, causing an undercut in the root of the supporting beam and affecting the integrity of the supporting beam. To cope with this situation, a structure to cancel the micro loading effect is designed, as shown in Fig. 2(b)[10]. Aluminum is splashed on a specified area of the glass substrate under the supporting beam and connected to the sil-

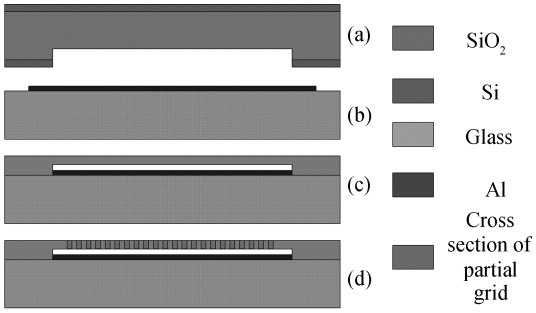

Fig. 7. Major fabrication process flow. (a) Silicon wafer with thermal SiO_2 is etched to form a suspending cavity. (b) Aluminum is splashed and patterned on Pyrex 7740 glass substrate. (c) Silicon–glass bonding and silicon thinning. (d) Deep RIE to release the proof mass.

icon proof mass. When the last layer of silicon is etched, the ions will hit the aluminum layers instead of the glass substrate, and the charge delivered by the ions will be released to the silicon proof mass, so the electrostatic bend force will disappear to free the supporting beam from the micro loading effect.

The fabricated accelerometer is shown in Fig. 8. Figure 8(b) shows that the integrity of the U-type beam is well maintained under the protection of the anti-micro loading structure; the damping comb in Fig. 8(c) is not only used to modify the damping feature of the accelerometer but also to protect the accelerometer from large shocks: when a large shock is applied on the x- or y-axis, the moving comb in the damping combs connects to the stator comb to avoid supporting beam damage.

The fabricated accelerometer and its static test equipment is shown in Fig. 9(a). The primary test shows that the sensitivity in the x- and y-directions is 0.53 pF/g and 0.49 pF/g respectively. The difference between the two axes may caused by over-etching in the DRIE process or the fact that the chip cannot be fully vertical with the static test equipment. Figures 9(b) and 9(c) shows the quality factor test of a single resonator with grid strip structure. The tested quality factor is 514, which proves that the grid strip structure has low damping. When the grid strip is used in the accelerometer design, the damping comb in Fig. 9(c) can be added to adjust the overall bandwidth and frequency response.

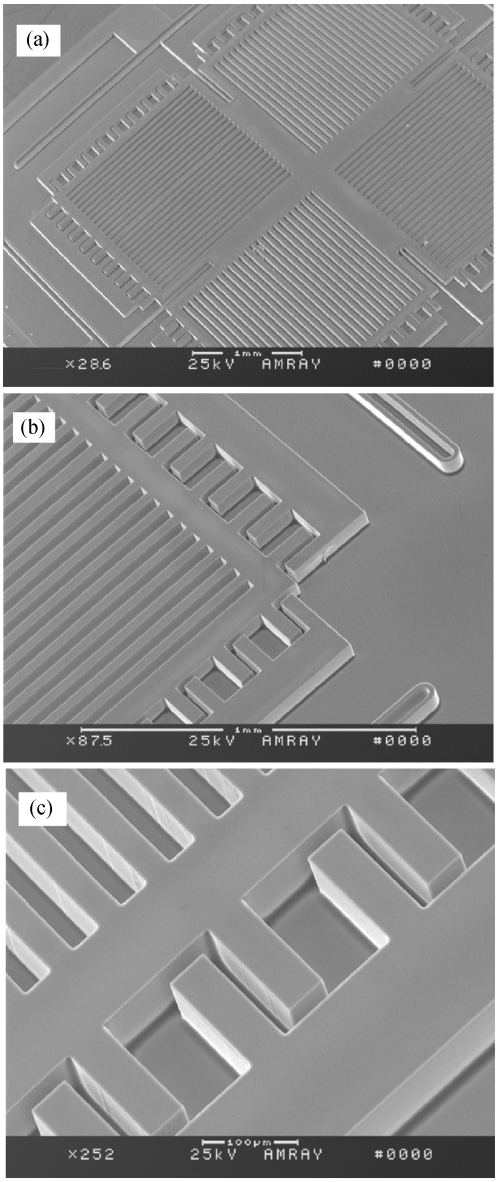

Fig. 8. SEM figures of the designed accelerometer. (a) Overall structure of the accelerometer. (b) U-type supporting beam. (c) Damping comb.

6. Conclusion

A capacitive MEMS biaxial accelerometer with grid strip structure is presented, which consists of grid strip sensing capacitors, supporting beams, connecting beams and aluminum electrodes etc. The accelerometer works on slide-film damping, which effectively reduces air damping and improves resolution. Damping combs are designed to adjust the overall bandwidth and frequency response.

FEM software, ANSYS, was employed to verify the correctness of the design. An anti-collision structure is designed in the x- and y-axes to avoid damage from large shocks; a strength analysis in the z-direction is performed which proves that the accelerometer can sustain a 1000 g shock in the z-axis; the transverse sensitivity is proved to be 0.

Electric-magnetic analyzing software, ANSOFT-Maxwell, was used to analyze the fringing electric field of the grid strip structure and its effects on the designed accelerometer. Analytical results show that a large error occurs when using the parallel plate approximation to calculate the capacitance of the grid strip structure; the capacitance sensitivity of the designed accelerometer decreases nonlinearly with the increase of proof mass displacement, and since the change rate is less than 0.3% within 5 μm displacement, it can be regarded as linear change; the capacitance increases with the increase of grid strip width under the same overlap width, but the growth rate decreases from 1.25% to 0.18%; the capacitance increases with the growth of grid strip thickness but when the thickness is above 70 μm the growth rate is very slow, which indicates that the thickness change caused by the non-ideal effect of the DRIE process can be neglected for the designed structure.

The designed accelerometer was fabricated based on deep RIE and silicon–glass bonding processes. A preliminary test was conducted which shows that the accelerometer has sensitivities of 0.53 pF/g and 0.49 pF/g on the x and y axes respec-

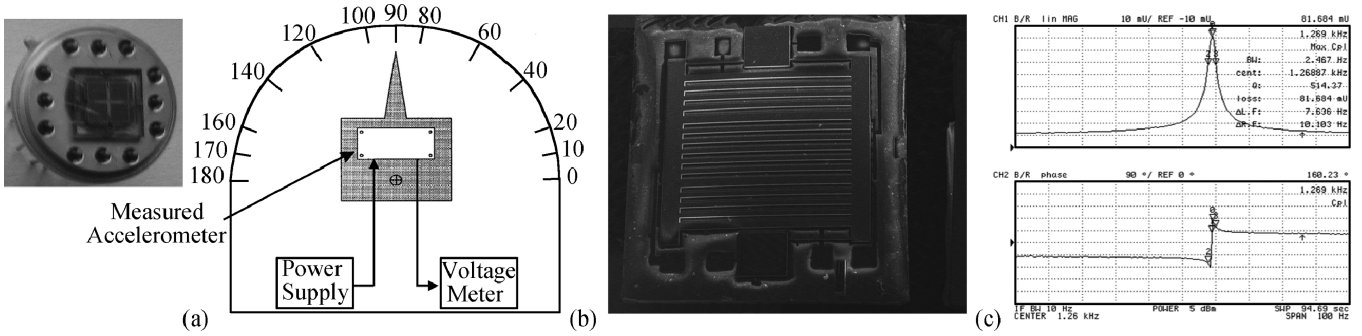

Fig. 9. Primary test of the accelerometer and Q-factor test of the grid strip resonator. (a) Sealed accelerometer chip and its static test. (b) Grid strip resonator. (c) The tested quality factor.

tively. A resonator with grid strip structure was fabricated and its quality factor is 514 in standard pressure, which proves that the grid strip structure can reduce the mechanical noise.

Acknowledgment

The authors wish to thank Professor Che Lufeng for his help on the testing interface circuit, and the State Key Laboratory of Transducer Technology of Shanghai Institute of Microsystem and Information Technology of Chinese Academy of Science for providing the fabrication facilities.

References

[1] Krishnamoorthy U, Olsson III R H, Bogart G R, et al. In-plane MEMS-based nano-g accelerometer with sub-wavelength optical resonant sensor. Sensors and Actuators A, 2008, 145/146: 283

[2] Dong Linxi, Che Lufeng, Wang Yuelin. The effect of non-parallel combs of the capacitive micro-sensor on the reliable operation range. Chinese Journal of Semiconductors, 2005, 26(2): 373

[3] Dong Linxi, Che Lufeng, Sun Lingling, et al. Effects of non-REF parallel combs on reliable operation conditions of capacitive inertial sensor for step and shock signals. Sensors and Actuators, 2005, 121(2): 395

[4] Li B, Lu D, Wang W. Micromachined accelerometer with area-changed capacitance. Mechatronics, 2001, 11: 811

[5] Dong Linxi, Yan Haixia, Qian Xian, et al. A novel capacitive bi-axial microaccelerometer based on the slide-film damping effect. Journal of Semiconductors, 2008, 29(2): 219

[6] Li Yong, Li Yuhe, Li Qingxiang, et al. Computation of electrostatic forces with edge effects for non-parallel comb-actuators. Tsinghua University (Sci & Tech), 2003, 43(8): 1024

[7] Gabrielson T B. Mechanical-thermal noise in micromachined acoustic and vibration sensors. IEEE Trans Electron Devices, 1993, 40(5): 903

[8] Gray P R, Meyer R G. Analysis and design of analog integrated circuits. 3rd ed. Wiley, 1977

[9] Petersen K E. Silicon as a mechanical material. Proc IEEE, 1982, 70: 420

[10] Chabloz M, Jiao J, Yoshida Y, et al. A method to evade microloading effect in deep reactive ion etching for anodically bonded glass–silicon structures. Proc IEEE Micro Electromechan Syst Workshop, Miyazaki, Japan, 2000